JOURNAL OF Materials CHEMISTRY

Formation mechanism of PMO with rope- and gyroid-based morphologies *via* close packing of secondary building units

S. S. Park, C. H. Lee, J. H. Cheon and D. H. Park*

Department of Chemistry, Inje University, 621-749 Kimhae, Kyungnam, Korea. Tel: +82 55 334 2073; Fax: +82 55 321 9718; E-mail: chempdh@ijnc.inje.ac.kr

Received 8th June 2001, Accepted 26th July 2001
First published as an Advance Article on the web 17th September 2001

Periodic mesoporous organosilicas (PMO) with a diversity of morphologies based on rope and gyroid shapes have been synthesized in one reaction batch. From the XRD pattern and TEM image, PMO with hexagonal symmetry was identified. Morphological investigations were carried out by SEM and TEM imaging. The generation of various morphologies could be interpreted partly in terms of the degree of curvature and the accretion type induced by various topological defects. The formation mechanism of PMO *via* the side-to-side close packing of platelet-, stick-, pin-, syringe-, and bullet-like particles as secondary building units was suggested.

Introduction

Since mesoporous silicas[1] using self-assembled surfactants as supramolecular templates were synthesized by the Mobil group in 1992, the surfactant mediated synthesis method has been applied to the preparation of a variety of mesoporous materials such as mesostructured oxides, sulfides, alumina, phosphates, metals and organic–inorganic hybrids.[2–19] The organic–inorganic hybrids are periodic mesoporous organosilicas (PMO) with organic groups covalently linked to Si inside the channel walls which have been derived by the sol–gel polymerization method.[20,21] The organic functionalization of the PMO framework opens up the possibility for many applications such as sensing, enantioselective separation, asymmetric syntheses, chromatographic supports and so on.[22–28]

Morphological control as well as handling and texture of mesoporous materials are extremely important for many applications. Mesoporous silicate materials with a variety of morphologies have been synthesized for many applications.[29–37] Recently, there have been reports of mesoporous materials with various particle shapes such as fibers, spheres, ropes, discoids, toroids, hollow tubes, and dodecahedra.[28,37–39] Reports of studies on the morphology and synthetic mechanism of PMO are limited. Cubic hybrid organic–inorganic mesoporous crystals with a dodecahedral shape, and hexagonal crystals with hexagonal rod and spherical shapes have been reported.[17,18] Lu *et al.* reported an evaporation-induced procedure for the formation of PMO films and spherical nanoparticles.[19] Ozin's group described a diversity of shapes and surface patterns that emerge from a surfactant-based synthesis of mesoporous silicas.[38] Different kinds of topological defects in seeds with liquid crystal-like properties affect the nucleation and growth of mesoporous materials, which lead to the formation of diverse morphologies with low and high curvature.[38,40] Although there have been some reports on the morphogenesis of mesoporous materials,[38,41,42] little is known about the formation of secondary building units as a constituent of mesoporous materials with various shapes and surface patterns.

In this study, we report that PMO with a range of morphologies based on rope and gyroid shapes may be synthesized through the accretion and packing of primary building units consisting of surfactant–organosilica co-assemblies and/or larger secondary building units with platelet-, pin-, syringe-, stick-, and bullet-like shapes. Using SEM and TEM images, we propose mechanisms for the formation of a wide range of shapes and surface patterns of PMO.

Experimental

Synthesis of ODTMA–PMO

Octadecyltrimethylammonium bromide (ODTMABr, from Aldrich, 100% purity) as a structure-directing surfactant and 1,2-bis(trimethoxysilyl)ethane (BTME, from Aldrich, 96%) as a precursor for periodic mesoporous organosilica were used. Sodium hydroxide (from Yakuri Co. Ltd, >99%), and absolute ethanol (from Hayman, 99.9% v/v) were purchased. All chemicals were used as purchased.

ODTMABr (0.634 g) was dissolved in gently heated water at the temperature of *ca.* 40 °C with stirring until a clear solution was obtained. Then, NaOH was added into the clear solution with stirring for a few minutes. Next, the solution was transferred into a Teflon bottle. BTME (0.944 ml) was added dropwise to the solution under vigorous stirring. After being stirred for 12 h, three portions of solution were placed in Teflon-lined autoclaves at 95 °C for 3 h, 6 h and 9 h, respectively. The molar composition of the final reaction mixture was 1.0 BTME : 0.57 ODTMABr : 2.36 NaOH : 353 H_2O. The solid products were recovered by filtration, washed with water, and dried at 60 °C. The surfactant was removed by a solvent extraction process, as follows. As-synthesized materials were stirred in 150 ml water containing 3 ml of 37 wt% HCl at 60 °C for 6 h, and the filtered solids were stirred with 150 ml of ethanol, refiltered, and dried at 60 °C. The samples obtained were designated as ODTMA–PMO.

Characterization

The material was characterized by X-ray diffraction, nitrogen adsorption–desorption measurements, scanning electron microscopy (SEM), and transmission electron microscopy (TEM). X-Ray powder diffraction patterns were obtained by using a Rigaku D/Max 2200 diffractometer using Cu K_α radiation. Nitrogen adsoption–desorption isotherms were measured at 77 K on a Micromeritics ASAP 2010 instrument. Surface areas

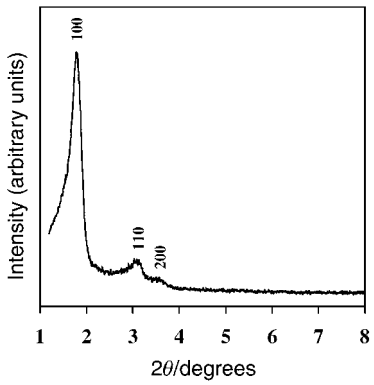

Fig. 1 XRD pattern of surfactant-extracted ODTMA–PMO synthesized at 95 °C for 9 h in a Teflon-lined autoclave.

were determined by the BET method and the pore size distribution curves were obtained using the BJH method from the desorption branch isotherms. ^{13}C and ^{29}Si cross polarization (CP) NMR spectra were recorded at room temperature on a Bruker DSX 400. SEM images were obtained using a KEVEX Sigma microscope with an acceleration voltage of 20 kV. The samples were coated with gold using a HITACHI E-1010 sputter coater prior to imaging. TEM images were obtained using a JEOL JEM-2010 microscope operating at 200 kV. Samples dispersed in ethanol were mounted on a carbon polymer microgrid supported on a copper grid, followed by drying at ambient conditions.

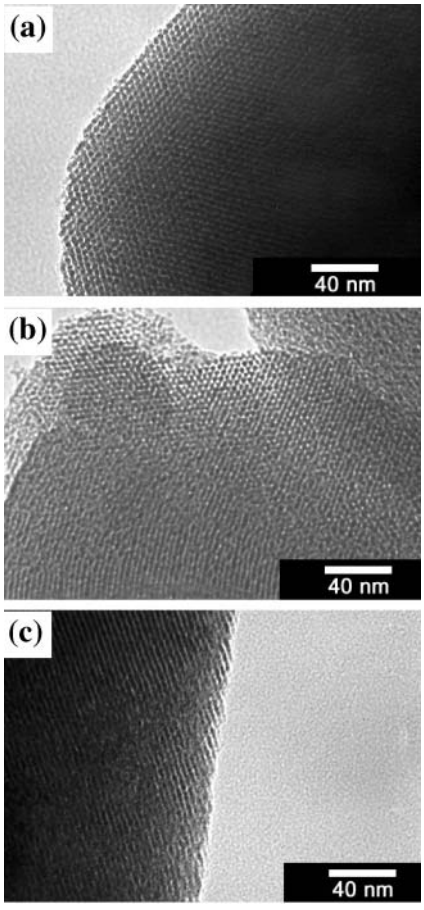

Fig. 2 TEM images of surfactant-extracted ODTAMA–PMO: (a) hexagonal basal plane with a well-ordered hexagonal array, (b) parallel curved surface channels run down the body length of the rope, and (c) surface channels of the twisted part run parallel on the tilt from the longitudinal axis of the rope.

Results and discussion

The periodic mesoporous organosilicas were synthesized by combining a solution of surfactant with a Si–C bonding source. The clear solution in a Teflon-lined autoclave was placed in an oven at an elevated temperature of 95 °C for 9 h. After extraction of the surfactant from the white powdered product, the XRD pattern of ODTMA–PMO was obtained and is shown in Fig. 1. The XRD pattern shows three resolved diffraction peaks that can be indexed as (100), (110) and (200) reflections of a hexagonal symmetry lattice, *p6mm*, with a hexagonal unit cell parameter $a_o \approx 53.4$ Å, which was determined from the 2θ value of the (100) peak of the XRD pattern.

Fig. 2 shows the TEM images of the hexagonal basal plane of the hexagonal rope (Fig. 2(a)) and the faceted bending parts that run down the hexagonal rope (Fig. 2(b)) of surfactant-extracted ODTMA–PMO. TEM images show well-ordered and regular hexagonal arrays of mesopores. Theses results are consistent with the XRD pattern. Fig. 3 shows the nitrogen adsorption–desorption isotherms and pore size distributions. The nitrogen adsorption–desorption isotherms show a type IV isotherm characteristic of mesoporous material. The sharp decrease of the desorption branch at 0.45 relative pressure indicates that the ODTMA–PMO consisted of uniform mesopores. The BET (Brunauer–Emmett–Teller) surface area was 769 $m^2\ g^{-1}$ and the pore diameter was 31 Å calculated by the BJH (Barrett–Joyner–Halenda) method.

The Si–C bonding in the framework was confirmed by ^{29}Si and ^{13}C CP MAS NMR experiments, as shown in Fig. 4. The ^{29}Si NMR spectrum shows two signal at −57.5 and −66.9 ppm which are assigned to partially condensed silicon, C(OH)-$Si(OSi)_2$ (T^2), and fully condensed silicon, $CSi(OSi)_3$ (T^3). The ^{13}C CP NMR spectrum is shown in Fig. 4. The ^{13}C NMR spectrum shows a strong single resonance at 5.2 ppm, which is attributed to carbon covalently linked to Si (Si–CH_2–CH_2–Si).

In order to investigate the morphological change of ODTMA–PMO during the hydrothermal reaction, the reaction time was varied. Fig. 5 shows SEM images of ODTMA–PMO synthesized at 95 °C for 3, 6, and 9 h, respectively. When synthesized at 95 °C for 3 h, long rope shaped and rope-based morphologies dominated and small particles with gyroid shapes formed, as shown in Fig. 5(a). As the reaction time increases, the proportion of gyroid particles increased. After 9 h of aging at 95 °C, gyroid shapes with larger sizes were observed, indicating that small gyroids grow gradually into large gyroids while the shape is retained. In addition to gyroid and rope shapes, worm-like aggregates were observed in the SEM images. Such long hexagonal ropes have rarely been observed in mesoporous silicate and organosilica materials.[23,37,43,44]

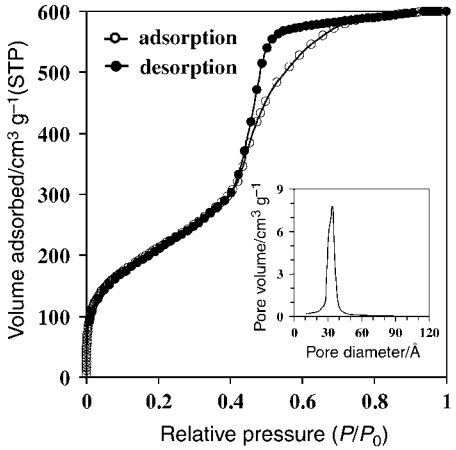

Fig. 3 Nitrogen adsorption–desorption isotherms for surfactant-extracted ODTMA–PMO. Inset shows the pore size distribution obtained using the desorption branch by the BJH method.

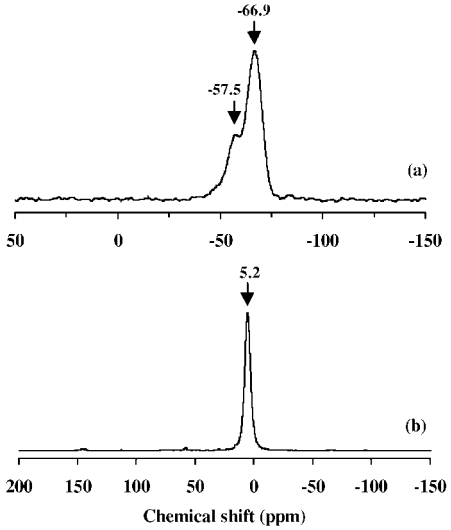

Fig. 4 (a) ^{29}Si and (b) ^{13}C cross-polarization (CP) MAS NMR spectra of surfactant-extracted ODTMA–PMO.

The hexagonal rope in Fig. 6(a) has a twisted and curved body and a hexagonal faceted surface along the longitudinal axis of the rope with a thickness of *ca.* 3 μm. The TEM image of the hexagonal basal plane, as shown in Fig. 2(a), shows a well-ordered hexagonal array, while parallel curved surface channels run down the body length of the rope, as shown in Fig. 2(b). These imply that the hexagonal ropes may be extended by accretion of surfactant–organosilica micelles on the basal plane. Growth toward the *c*-axis of the hexagonal unit induces the formation of longer ropes. The terminal part sometimes exhibits dislocation of the hexagonal platelets that seem to be the building units of the rope structure, as shown in Fig. 6(a). The degree of dislocation seems to depend on the degree of rope curvature, the thickness of the stacking platelets and the degree of attraction force between the hexagonal faces of neighboring platelets. By varying the degree of curvature, affected by topological defects of the seed crystals, periodic mesoporous organosilicas with spiral (Fig. 6(b)–(e)), toroid (Fig. 6(f)), and discoid morphologies (Fig. 6(g)) based on the rope structure are produced. Assuming that the packing geometry of the flexible rod-like micelles in the organosilicate liquid crystal seed is hexagonal, the formation of mesoporous organosilicas with various rope-based shapes may be partly explained using some kind of dislocation or disclination defects pertinent to the organosilicate liquid crystal seed. Bending of the rope may be initiated from a disclination rotated along the

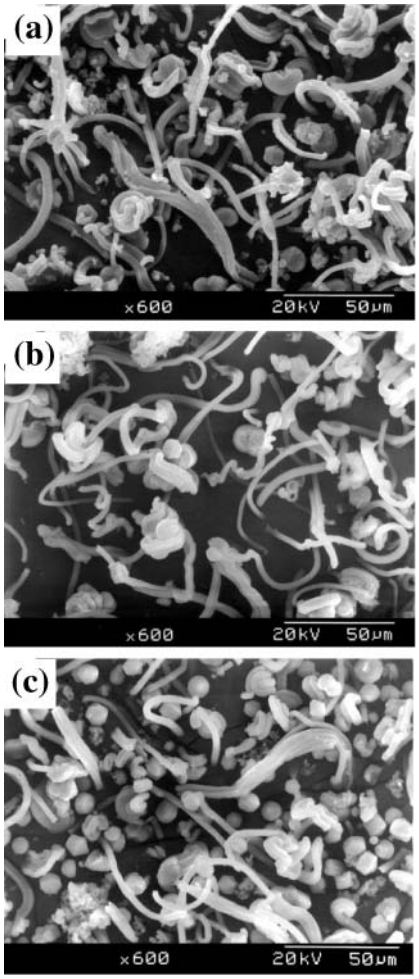

Fig. 5 SEM images of ODTMA–PMO synthesized at 95 °C for (a) 3 h, (b) 6 h, and (c) 9 h in a Teflon-lined autoclave.

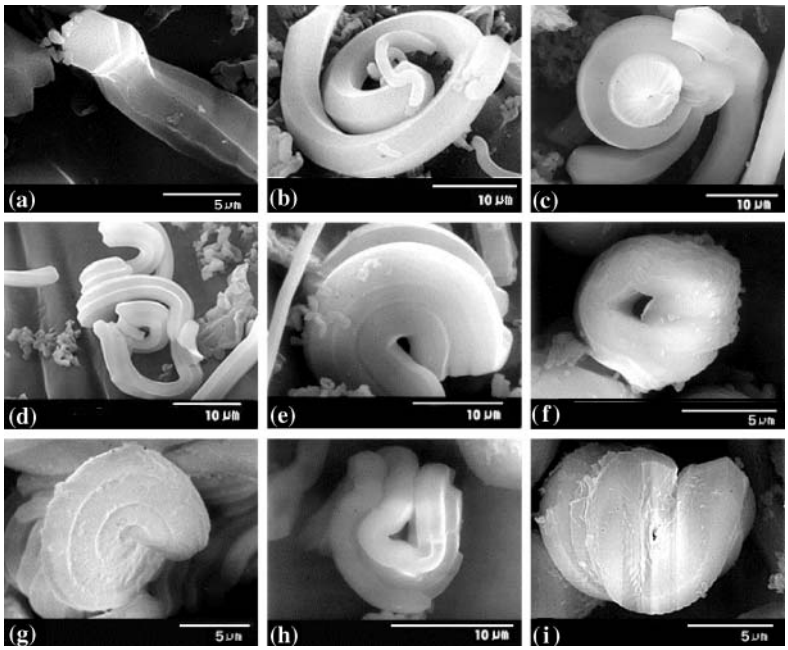

Fig. 6 SEM images of particles with rope and rope-based morphologies.

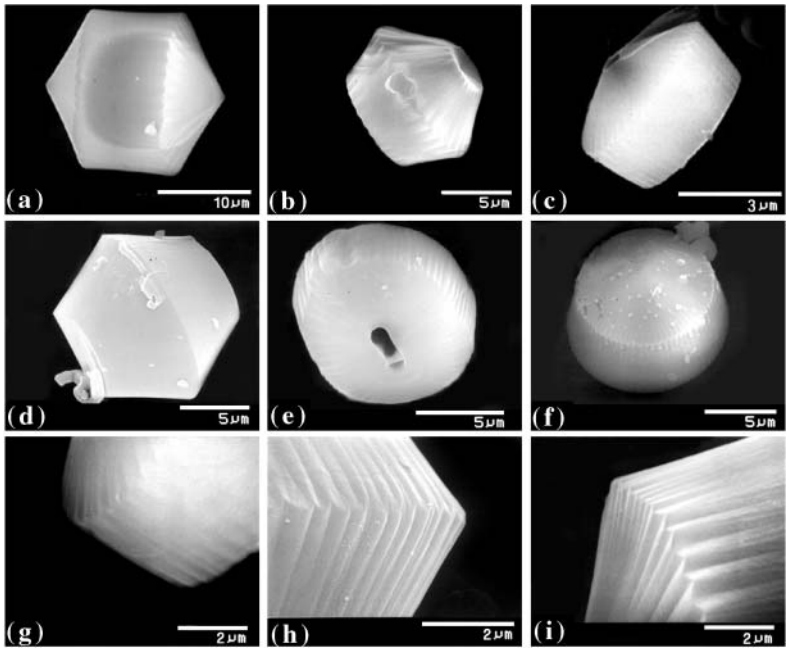

Fig. 7 (a)–(f) SEM images of PMO with various symmetric gyroid morphologies, and (g)–(i) magnified images of the edge of the gyroids.

transverse axis and twisting may result from a disclination around the longitudinal axis. While the parallel curved surface channels of faceted bending parts of the hexagonal rope run down the body length of the rope (Fig. 2(b)), the surface channels of twisted parts run parallel to the tilt from the longitudinal axis of the rope (Fig. 2(c)). This indicates that disclinations about the transverse axes alter the pore orientation, while disclinations about the longitudinal axes alter the rotational configuration of the array. Complex structures based upon a combination of two defects can lead to a variety of

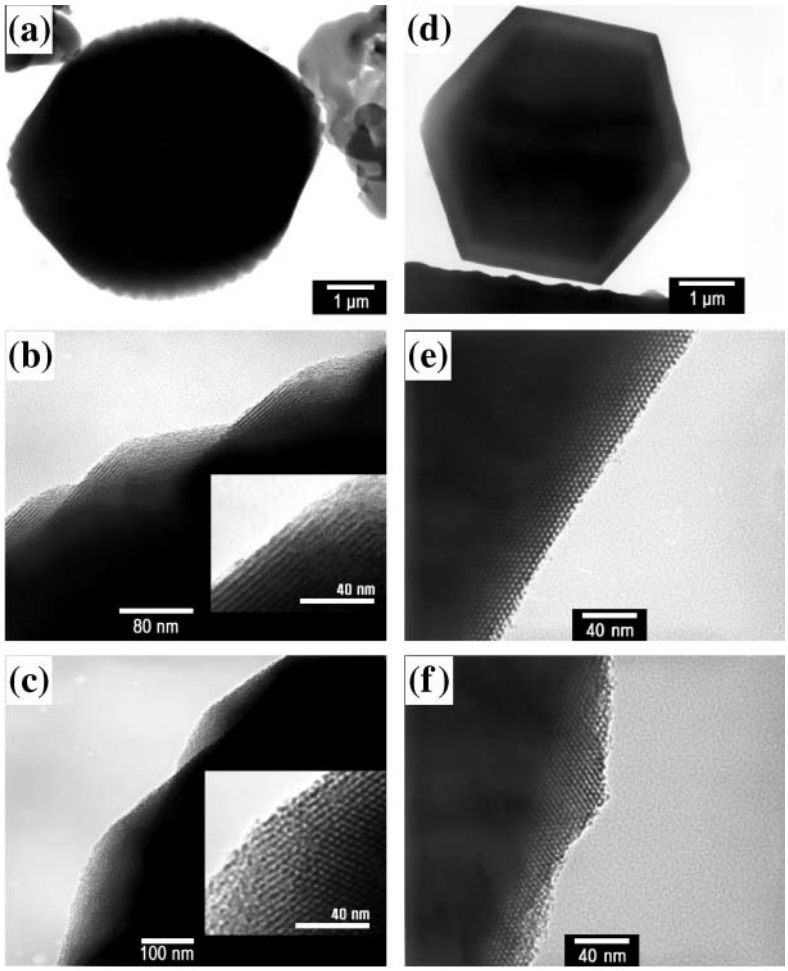

Fig. 8 (a) and (d) TEM images of two differently shaped gyroids, and magnified images of (b) top and (c) left edges of gyroid (a), and (e) edge and (f) vertex part of gyroid (d).

morphologies (Fig. 6(h) and (i)). This approach could be adopted to interpret remarkable morphologies of periodic mesoporous organosilicas, although the wall properties of periodic mesoporous organosilicas are distinguished from those of mesoporous silica MCM-41 due to the organic moieties within the framework.

Fig. 7 shows the SEM images for PMOs with symmetric gyroid morphology, the different shapes depending on a range of reaction variables in one reaction batch. These materials have regular surface patterns with a few hundred nanometer between successive patterns. These symmetric morphologies and regular surface patterns generated by inorganic–organic hybrids may be related to biomineralization, in which organic materials play an important role in the organization of the inorganic material.

Fig. 8(b) and (c) show the TEM images for the top and side edges, respectively, of the gyroid shown in Fig. 8(a) which have a regular surface pattern. The channels corresponding to hexagonal arrays of mesopores based on the (100) and (110) reflections, respectively, are arrayed with a regular orientation on the surface of repetitive humps. From the magnified TEM images shown in insets in Fig. 8(b) and (c), the highly ordered hexagonal mesostructure of a gyroid can be verified. Fig. 8(e) and (f) show the TEM images for the edge and vertex parts, respectively, of the differently shaped gyroid shown in Fig. 8(d). The edge part, as shown in Fig. 8(e), has a well-ordered hexagonal mesostructure without humps, while the vertex part is humped, as shown in Fig. 8(f).

On the basis of the SEM and TEM images, the following mechanism for the formation of various morphologies and surface patterns in the synthesis of periodic mesoporous organosilica is suggested. As suggested by Ozin's group, the hexagonal cylindrical liquid crystal seeds are formed through the self-assembly of surfactant-based micelles with polymerized organosilica and, then, a variety of spiral and gyroid morphologies are formed through the repetitive accretion of organosilica–micellar co-assembled species with varying degrees of curvature and linear topological defects.[38,41,45] As the organosilica–surfactant co-assembly grows about a fixed axis and simultaneously rigidifies into PMO with gyroid morphology, the smooth surface and/or finely superimposed surface patterns appear, as shown in the magnified SEM images of well-ordered surface patterns (Fig. 7(g)–(i)).

As particles composed of building units such as enlarged platelet-, pin-, stick-, syringe-, and bullet-like shapes, as shown in Fig. 9 and 10, have been found, the growth mechanism of PMO *via* micrometer-sized secondary building blocks is tentatively suggested. The organosilica–micellar co-assembled species designated as primary building units grow to become the enlarged platelet-, pin-, stick-, syringe-, and bullet-like shapes designated as secondary building units. Fig. 9(a) shows the SEM image of a particle with a surface pattern consisting of furrows and ridges resulting from whirling of successively dislocated platelets. The shape of the particle shown in Fig. 9(b) appears to have been formed by filling the furrows on the particle consisting of pin-shaped units in Fig. 9(a) with organosilica–micellar co-assembled species of smaller size. As shown in Fig. 9(c), pin-shaped units are arranged into a concentric circle and packed closely. Moreover, syringe-like shaped units make another layer with the oriented attachment of the sharp end part of the syringe to the surface. As shown in Fig. 10(a) and (b), bullet- and stick-like particles with length *ca.* 5 μm are lined up vertically, and arranged alternately up and down. Fig. 10(c) shows another packing type by arrangement

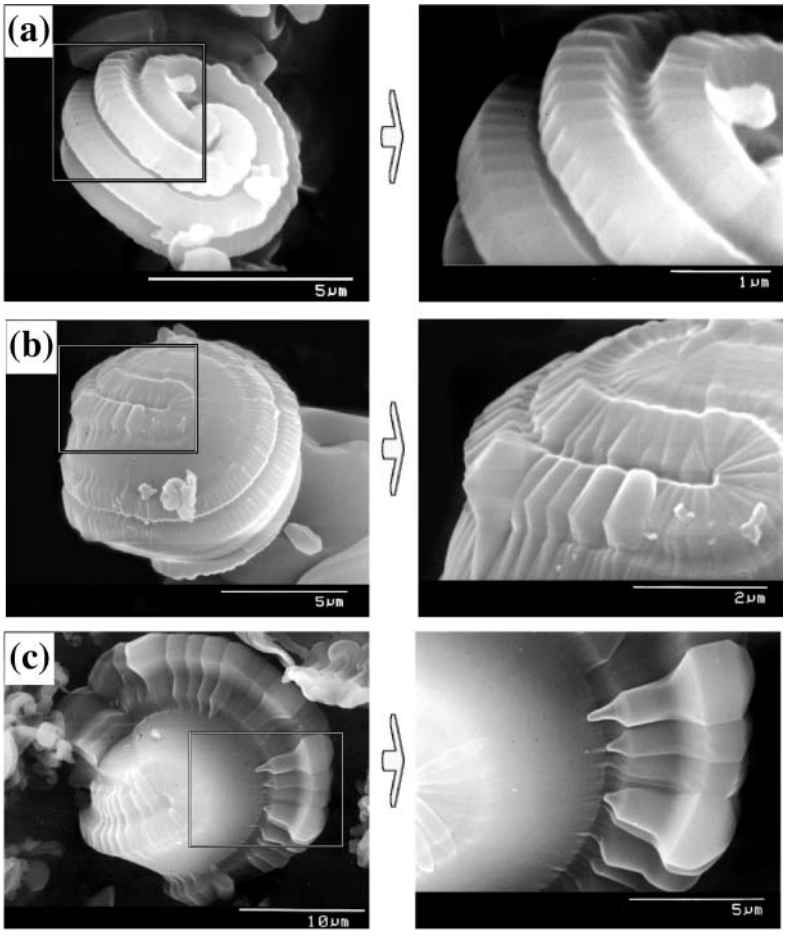

Fig. 9 SEM images of particles consisting of (a) platelet-, (b) pin-, and (c) syringe-like shaped units. Magnified images of the sections marked with boxes in (a)–(c) are shown on the right-hand side, respectively.

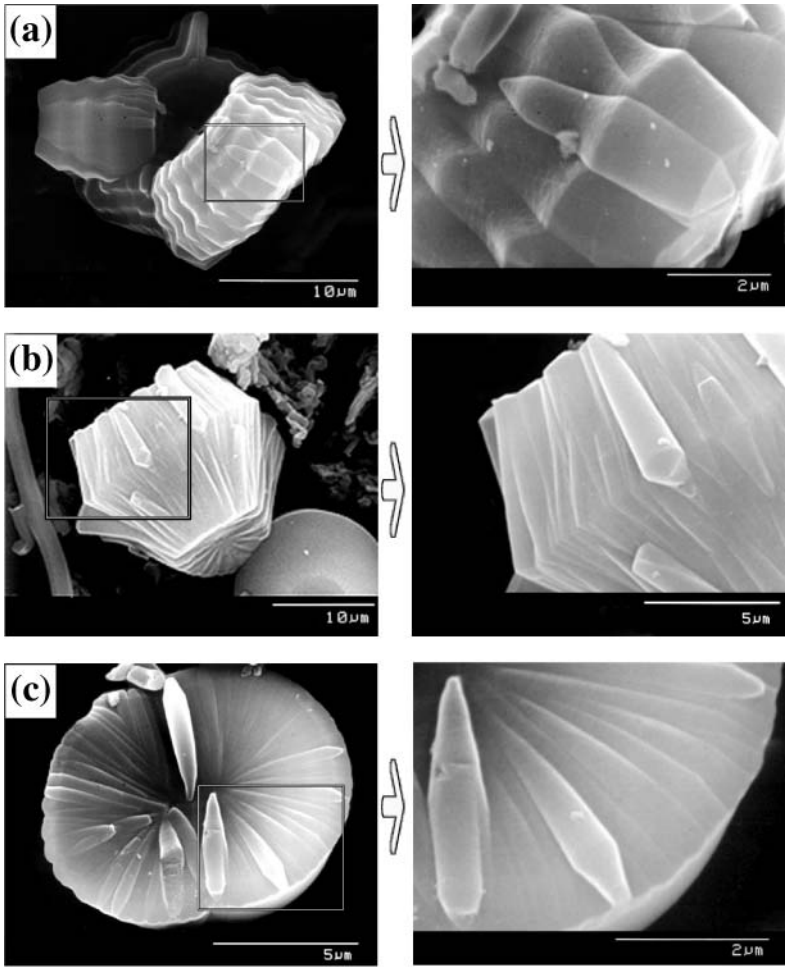

Fig. 10 SEM images of particles consisting of (a) bullet- and (b) stick-like shaped units, respectively and (c) SEM of particle formed through concentric circling of stick-like units. Magnified images of the sections marked with boxes in (a) and (b) are shown on the right-hand side, respectively.

of concentric circles of stick-like particle. These enlarged units with a variable packing parameter are assembled and stabilized due to the reduction of the surface free energy, which leads to the formation of particles with distinct surface patterns with wider spaces between successive patterns. It seems that this structure will minimize the repulsion between building layers, and facilitate the stacking of layers. Thus, gyroid-based shapes with high curvature can be also formed through stacking of these units. Thus, the gyroid would exhibit vertically wrinkled surface patterns. As described above, the results present strong evidence that the secondary building units (platelet-, pin-, stick-, syringe-, and bullet-like shapes) are packed by side-to-side growth, which may result in the formation of various shapes with high curvature.

Conclusions

Hybrid inorganic–organic mesoporous materials with hexagonal symmetry were synthesized using ODTMABr as a templating surfactant, and BTME as the Si–C bonding source. At the initial stages of the reaction, rope and rope-based shapes were preferentially formed. After reaction for 9 h, large gyroids as well as longer ropes were formed. The generation of various morphologies could be interpreted partly in terms of the degree of curvature and the accretion type induced by various topological defects. Also, the mechanism for the formation and growth of gyroid morphology *via* secondary building units such as platelet-, pin-, stick-, syringe-, and bullet-like shapes is suggested using SEM and TEM images.

Acknowledgements

This study was supported by the academic research fund (BK21, HEKSIM D0024) of the Ministry of Education, Republic of Korea.

References

1 C. T. Kresge, M. E. Leonowitz, W. J. Roth, J. C. Vartuli and J. S. Beck, *Nature*, 1992, **359**, 710.
2 U. Ciesla, S. Schacht, G. D. Stucky, K. K. Unger and F. Schüth, *Angew. Chem., Int. Ed. Engl.*, 1996, **35**, 541.
3 P. V. Bran, P. Osenar and S. I. Stupp, *Nature*, 1996, **380**, 325.
4 S. A. Bagshaw and T. J. Pinavaia, *Angew. Chem., Int. Ed. Engl.*, 1996, **35**, 1102.
5 Q. Huo, D. I. Margolese, U. Ciesla, P. Feng, T. E. Gier, P. Sieger, R. Leon, M. Petroff, F. Schüth and G. D. Stucky, *Nature*, 1994, **368**, 317.
6 D. M. Antonelli and J. Y. Ying, *Angew. Chem., Int. Ed. Engl.*, 1996, **35**, 325.
7 M. J. MacLachlan, N. Coombs and G. A. Ozin, *Nature*, 1999, **397**, 681.
8 Z. R. Tian, W. Tong, J. Y. Wang, N. G. Duan, V. V. Krishnan and S. L. Suib, *Science*, 1997, **276**, 926.
9 G. S. Attard, P. N. Bartlett, N. R. B. Coleman, J. M. Elliott, J. R. Owen and J. H. Wang, *Science*, 1997, **278**, 838.
10 Q. Luo, L. Li, Z. Xue and D. Zhao, *Stud. Surf. Sci. Catal.*, 2000, **129**, 37.
11 M. Yada, H. Hiyoshi, K. Ohe, M. Machida and T. Kijima, *Inorg. Chem.*, 1997, **36**, 5565.
12 S. Inagaki, S. Guan, Y. Fukushima, T. Ohsuna and O. Terasaki, *J. Am. Chem. Soc.*, 1999, **121**, 9611.
13 T. Asefa, M. J. MacLachlan, N. Coombs and G. A. Ozin, *Nature*, 1999, **402**, 867.

14 B. J. Melde, B. T. Holland, C. F. Blanford and A. Stein, *Chem. Mater.*, 1999, **11**, 3302.
15 T. Asefa, M. J. MacLachlan, H. Grondley, N. Coombs and G. A. Ozin, *Angew. Chem., Int. Ed.*, 2000, **39**, 1808.
16 C. Yoshina-Ishii, T. Asefa, N. Coombs, M. J. MacLachlan and G. A. Ozin, *Chem. Commun.*, 1999, 2539.
17 S. Guan, S. Inagaki, T. Ohsuna and O. Terasaki, *J. Am. Chem. Soc.*, 2000, **122**, 5660.
18 A. Sayari, S. Hamoudi, Y. Yang, I. L. Moudrakovski and J. R. Ripmeester, *Chem. Mater.*, 2000, **12**, 3857.
19 Y. Lu, H. Fan, N. Doke, D. A. Loy, R. A. Assink, D. A. LaVan and C. J. Brink, *J. Am. Chem. Soc.*, 2000, **122**, 5258.
20 R. H. Baney, M. Itoh, A. Sakakibar and T. Suzuki, *J. Chem. Rev.*, 1995, **95**, 1409.
21 D. A. Log and K. J. Shea, *J. Chem. Rev.*, 1995, **95**, 1431.
22 T. Lee, N. Yao and I. A. Aksay, *Langmuir*, 1997, **13**, 3866.
23 (*a*) I. A. Aksay, M. Trau, S. Manne, I. Honma, N. Yao, L. Zhou, P. Fenter, P. M. Eisenberger and S. M. Gruner, *Science*, 1996, **273**, 892; (*b*) S. Schächt, Q. Huo, I. G. Boigt-Martin, G. D. Stucky and F. Schüth, *Science*, 1996, **273**, 768.
24 (*a*) S. Mann and G. A. Ozin, *Nature*, 1996, **382**, 313; (*b*) S. A. Davis, S. L. Burkett, N. H. Mendelson and S. Mann, *Nature*, 1997, **385**, 420.
25 D. Zao, J. Feng, Q. Huo, N. Melosh, G. H. Fredrickson, B. F. Chmelka and G. D. Stucky, *Science*, 1998, **279**, 548.
26 D. Zao, Q. Huo, J. Feng, B. F. Chmelka and G. D. Stucky, *J. Am. Chem. Soc.*, 1998, **120**, 6024.
27 Q. Huo, D. I. Margolese, U. Ciesla, J. Feng, T. E. Gier, P. Sieger, R. Leon, P. M. Petroff, F. Schüth and G. D. Stucky, *Nature*, 1994, **368**, 317.
28 M. Trau, N. Yao, E. Kim, Y. Xia, G. M. Whitesides and I. A. Aksay, *Nature*, 1997, **390**, 674; H. Yang, N. Coombs and G. A. Ozin, *Adv. Mater.*, 1997, **9**, 811.
29 P. T. Tanev, Y. Liang and T. J. Pinnavaia, *J. Am. Chem. Soc.*, 1997, **119**, 8616.
30 P. T. Tanev and T. J. Pinnavaia, *Science*, 1996, **271**, 1267.
31 S. H. Tolbert, T. E. Schäffer, J. Feng, P. K. Hansma and G. D. Stucky, *Chem. Mater.*, 1997, **9**, 1962.
32 Q. Huo, D. Zhao, J. Feng, K. Weston, S. K. Buratto, G. D. Stucky, S. Schächt and F. Schüth, *Adv. Mater.*, 1997, **9**, 974.
33 P. Yang, T. Deng, D. Zhao, P. Feng, D. J. Pine, B. F. Chmelka, G. M. Whitesides and G. D. Stucky, *Science*, 1998, **282**, 2244.
34 S. S. Kim, W. Zhang and T. J. Pinnavaia, *Science*, 1998, **282**, 1302.
35 Q. Huo, J. Feng, F. Schüth and G. D. Stucky, *Chem. Mater.*, 1997, **9**, 14.
36 S. M. Yang, H. Yang, N. Coombs, I. Sokolov, C. T. Kresge and G. A. Ozin, *Adv. Mater.*, 1999, **11**, 52.
37 P. J. Bruinsma, A. Y. Kim, J. Liu and S. Baskaran, *Chem. Mater.*, 1997, **9**, 2507.
38 H. Yang, N. Coombs and G. A. Ozin, *Nature*, 1997, **386**, 692.
39 S. Oliver, A. Kuperman, N. Coombs, A. Lough and G. A. Ozin, *Nature*, 1995, **378**, 47.
40 Y. Bouligand, *J. Phys.*, 1980, **41**, 1297.
41 O. Regev, *Langmuir*, 1996, **12**, 4940.
42 M. Yada, H. Hitosh, K. Ohe, M. Machida and T. Kijima, *Inorg. Chem.*, 1997, **36**, 5565.
43 D. Zhao, J. Sun, Q. Li and G. D. Stucky, *Chem. Mater.*, 2000, **12**, 275.
44 G. Schulz-Ekloff, J. Rathousky and A. Zukal, *Microporous Mesoporous Mater.*, 1999, **27**, 273.
45 Y. S. Lee, D. Surjadi and J. F. Rathman, *Langmuir*, 1996, **12**, 6202.